

Article

# Tip Vortex Cavitation and Induced Noise Characteristics of Hydrofoils

Suyong Shin <sup>1,2,†</sup>, Ji-Woo Hong <sup>2,†</sup>, David Nagarathinam <sup>2,†</sup>, Byoung-Kwon Ahn <sup>2,\*</sup> and Sung-Gun Park <sup>1</sup>

<sup>1</sup> Structure/Vibration & Noise, R&D Department, Daewoo Shipbuilding and Marine Engineering, Geoje-si 3370, Korea; syshin09@dsme.co.kr (S.S.); sgspark8@dsme.co.kr (S.-G.P.)

<sup>2</sup> Department of Naval Architecture and Ocean Engineering, Chungnam National University, Daejeon 34134, Korea; hggp02@naver.com (J.-W.H.); davidnresearch@gmail.com (D.N.)

\* Correspondence: bkahn@cnu.ac.kr; Tel.: +82-42-821-6625

† These authors contributed equally to this work.

**Abstract:** Tip vortex cavitation is one of the most classical themes in fluid mechanics. Although many experimental and theoretical studies have been performed, unsolved problems still remain. In particular, the trailing vortices at the tip of the hydrofoil directly affects the hydrodynamic and acoustic performance of submerged objects such as the marine propeller, rudder and various foil-shaped appendages of the ship. In this study, the experimental results from the measurements of the vortex cavitation from the tip of two different three-dimensional hydrofoils are presented. Experiments have been carried out in Chungnam National University-Cavitation Tunnel (CNU-CT). By high speed imaging technique, the development process of vortex cavitation is observed in detail. Based on the high-speed images, physical features of the cavity inception and the swirling motion of the tip vortex cavity flow are examined. In addition, the induced noise characteristics in the vortex development process are examined by unsteady pressure measurements. The forces exerted on the hydrofoil were also measured using a dynamometer with a view to verify the scaling relation between the inception cavitation number and the non-dimensional parameters namely, the coefficient of lift,  $C_L$  and the Reynolds number,  $Re$ . The results further shed light on the cause of the intense noise induced by tip vortex cavitation.

**Keywords:** hydrofoil; cavitation; cavity inception; tip vortex cavitation (TVC); sound pressure level (SPL)



**Citation:** Shin, S.; Hong, J.W.; Nagarathinam, D.; Ahn, B.K.; Park, S.G. Tip Vortex Cavitation and Induced Noise Characteristics of Hydrofoils. *Appl. Sci.* **2021**, *11*, 5906. <https://doi.org/10.3390/app11135906>

Academic Editors: Florent Ravelet and Francesca Scargiali

Received: 25 May 2021

Accepted: 22 June 2021

Published: 25 June 2021

**Publisher's Note:** MDPI stays neutral with regard to jurisdictional claims in published maps and institutional affiliations.



**Copyright:** © 2021 by the authors. Licensee MDPI, Basel, Switzerland. This article is an open access article distributed under the terms and conditions of the Creative Commons Attribution (CC BY) license (<https://creativecommons.org/licenses/by/4.0/>).

## 1. Introduction

Tip vortex cavitation has been documented since the early works of Sir Charles Parsons [1] in the year 1895, with photographs in a cavitation tunnel. Wing-tip vortices are characterized by large swirling motion along the axial direction, low-pressure in the core region and large turbulent fluctuations in the vortex center [2,3]. Peng [2] performed Laser Doppler Velocimetry (LDV) and Stereo Particle Imaging Velocimetry (SPIV) in a flow over an elliptical hydrofoil with National Advisory Committee for Aeronautics (NACA) hydrofoil section, namely NACA 16-020 and observed large magnitudes of vorticity and large gradients of tangential velocity about the vortex core. By numerical computations, Jeong [3] showed large vorticity magnitudes and low pressure regions in the core of the vortex behind an elliptic NACA 16-020 elliptic hydrofoil of a finite aspect ratio. Fruman [4] explained the effects of wing planform on the vortex features observed in the leeward side of the wing and the cavitation in the low-pressure vortex core in their experiments. The low pressure vortex core in the leeward side of the hydrofoils undergo cavitation once the pressure in the vortex core falls below a critical value called vapor pressure at its corresponding fluid temperature [5]. Finding the conditions when cavitation inception happens has attracted the attention of many researchers [6]. Based on empirical scaling laws, Astolfi [7] showed the viscosity and the vortex strength to be crucial in determining

the cavitation inception. The effects of water quality in determining the cavitation inception has been studied experimentally by Arndt [8]. Briancon [9] showed the effects of dissolved oxygen percentage and measured water quality in determining the cavitation inception and noise characteristics of a cavitating NACA 0020 hydrofoil experimentally. Cavitation inception number for any hydrofoil section has been shown to be related to its angle of the inclination and the Reynolds number of the flow by semi-empirical observations by McCormick [10]. Souders [11], Billet [12] and maines [13] have further experimentally verified the validity of McCormick's power-law scaling relation for the cavitation inception number. Velocity and length scale effects on the cavitation inception number has also been shown experimentally by Billet [12]. Experimentally, Keller [14] has shown the velocity, length, viscous and turbulence scaling effects on the cavitation inception number. He also showed the effects of water quality in determining the cavitation inception number.

A unique, strong frequency associated with the cavitating hydrofoil, called "singing" was shown experimentally by Higuchi [15] using hydrophone measurements in an elliptic planform hydrofoil in a cavitation tunnel. Maines [16] showed that the "singing" occurred over a range of cavitation numbers at a given coefficient of lift. Choi [17] showed a correlation between the deformation of bubble nucleus and the noise generated in tip vortex cavitation. Pennings [18] and Peng [19] have shown the sharp noise associated with the tip vortex cavitation in their laboratory experiments. In the current study, the cavitation inception and the noise characteristics of NACA 16-020 and NACA 66(2)-415 hydrofoils are studied using high speed imaging and unsteady pressure measurements. Novelty of the current work is in simultaneous comparison of the high-speed images with the unsteady pressure spectrum at each stage of the cavity evolution with the decrease of the cavitation number.

## 2. Experimental Setup

Experiments were carried out at the cavitation tunnel of the Chungnam National University (CNU-CT). The size of the test section is 100 mm × 100 mm × 1400 mm (H × B × L), and the maximum flow speed is 20 m/s. Pressure inside the tunnel can be changed from 10 to 300 kPa. Figure 1 shows the schematic of the experimental setup. Two hydrofoils of elliptic planform with different cross-sections, NACA 16-020 and 66(2)-415, were tested. Aspect ratio of the foil is 1.5 and the length of the chord and span is 80 mm and 60 mm respectively. The cavitating hydrofoil was imaged using a high speed camera, capturing videos at the rates up to 80,000 fps at the resolution of 1280 × 1024 pixels on a complementary metal–oxide–semiconductor (CMOS) sensor. Minimum exposure time of the camera shutter is 3.9 µs. Forces exerted on a hydrofoil were measured by using a dynamometer. The three-component dynamometer is capable of measuring forces along two perpendicular directions and moment along one direction. The dynamometer is capable of force measurement up to 20 kgf along the streamwise direction and 50 kgf along the cross-stream direction. Maximum moment measurable is 1 kgf.m about the perpendicular. The dynamometer was calibrated before measurements and linear response curve was obtained for their operating range. The dynamometer also exhibited no hysteresis and had a good repeatability; performance characteristics of the dynamometer is tabulated in Table 1. The pressure fluctuations were measured at the top of the test section and analyzed in the frequency domain according to the test conditions. The unsteady pressure transducer used in the experiments can measure absolute pressure up to 2 bar at the sampling rate of 50,000 Hz. A customized LABVIEW interface was utilized to operate the cavitation tunnel, record the high-speed images, obtain the voltage output of the dynamometer and the unsteady pressure signals from the pressure transducer in a synchronous manner. The key parameter is the cavitation number,  $\sigma = (P_\infty - P_v)/(1/2\rho V_\infty^2)$ , where,  $P_\infty$ ,  $P_v$ ,  $\rho$ ,  $V_\infty$  are the free-stream wall static pressure measured at the test section entrance, water vapor pressure at the fluid temperature, water density and flow speed respectively.

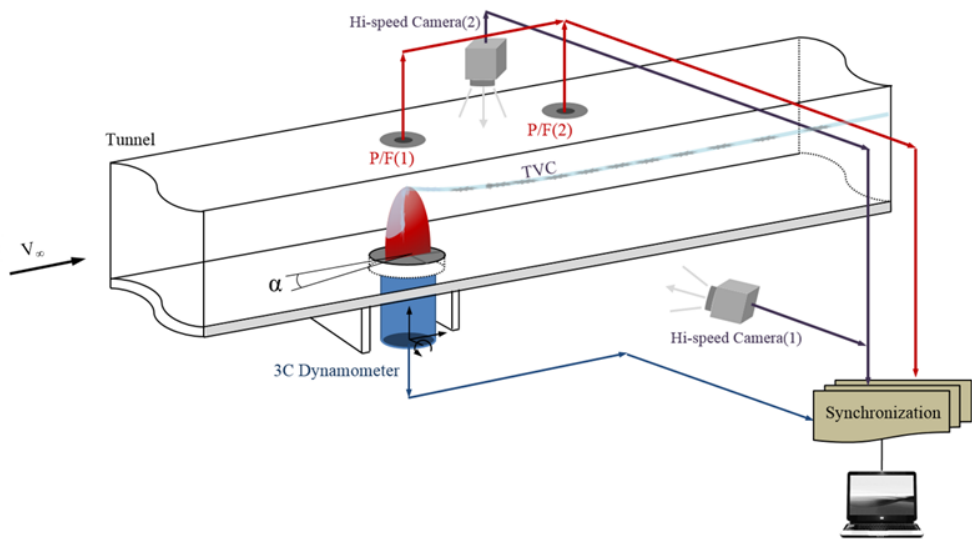


**Figure 1.** Schematic of the experimental set-up. Three component dynamometer, high speed cameras and the wall-mounted pressure transducers are synchronized via a LABVIEW interface.

**Table 1.** Performance characteristics of the dynamometer.

	Capacity	Linearity [%]	Hysteresis [%]	Repeatability [%]
$F_x$	20 kgf	0.623 mVolt/Volt	-0.01	-0.03
$F_y$	50 kgf	1.559 mVolt/Volt	0.01	-0.04
$M_z$	1 kgf.m	0.874 mVolt/Volt	-0.01	0.05

### 3. Results and Discussion

#### 3.1. Cavitation Inception

The cavitation inception for the NACA 16-020 hydrofoil at the angle of inclination of  $15^\circ$  and cavitation number,  $\sigma = 2.97$  is shown in Figure 2. Cavitation inception is characterized by streaks of water vapor pocket along the low pressure vortex core trailing downstream of the NACA 16-020 hydrofoil. Such sporadic streaks of varying lengths and time periods are noticeable along the vortex core, once the cavitation inception happens. Water vapor bubble pockets of varying lengths get advected along the vortex core sporadically, once the cavitation inception happens and they are encircled in Figure 2. The attached cavitation inception for the NACA 66(2)-415 hydrofoil at the angle of inclination of  $\alpha = 8^\circ, \sigma = 2.14$  is shown in Figure 3 by an arrow. The attached tip vortex is discretely identifiable by a continuous line from the tip of the vortex, advecting downstream. The area of the water vapor bubble streaks advecting sporadically at irregular time intervals along the vortex core was measured by binarizing the RGB images once the cavitation inception was noticed. The cavity area obtained from the high-speed imaging with time is given in Figure 4 for NACA 16-020 hydrofoil at  $\alpha = 15^\circ, \sigma = 2.97$  as red curve and for NACA 66(2)-415 hydrofoil at  $\alpha = 8^\circ, \sigma = 2.14$  as a green curve. The cavity area and the time period associated with the cavity inception is sporadic in nature as observed by the time series in Figure 4.

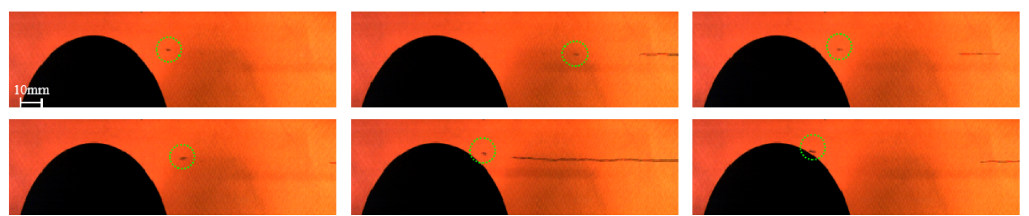


**Figure 2.** Inception of tip vortex cavitation NACA 16-020,  $\alpha = 15^\circ$ ,  $\sigma = 2.97$ .



**Figure 3.** Fully developed inception of tip vortex cavitation NACA 66(2)-415,  $\alpha = 8^\circ$ ,  $\sigma = 2.14$ .

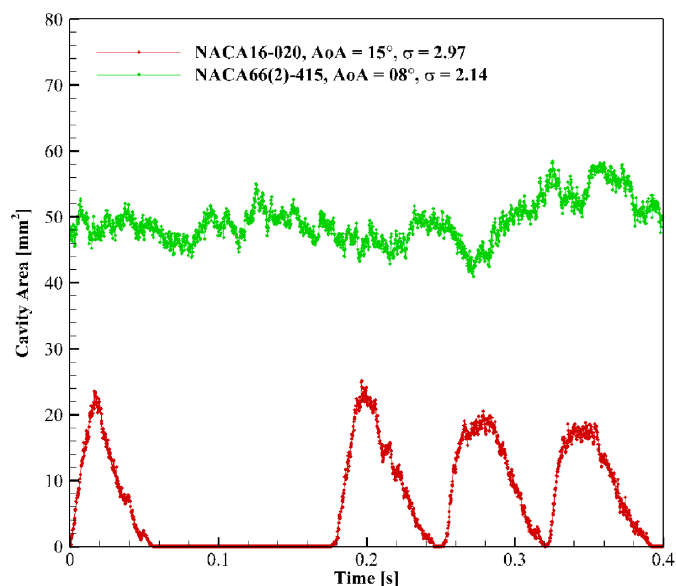


**Figure 4.** Cavity area variation with time for NACA 16-020 at the instance of cavity inception,  $\alpha = 15^\circ$ ,  $\sigma = 2.97$  and for NACA 66(2)-415 at the instance of cavity inception,  $\alpha = 8^\circ$ ,  $\sigma = 2.14$ .

Finding the cavitation inception number for various hydrofoils under various angles of incidence and Reynolds number is an important step in the cavitation inception prediction. In order to derive an expression for the cavitation inception number, we summarize the derivation given by McCormick [10] here below by considering the radial equilibrium of a fluid element swirling about the vortex axis. Let us consider a fluid element of mass  $dm$ , swirling at the rotation rate,  $\omega$  at a distance  $r$  from the vortex axis. The force balance on the fluid element is shown in Figure 5.

$$(P + dp)(r + dr)d\theta - Prd\theta = dm \frac{v_\theta^2}{r}, \quad (1)$$

$$\frac{\partial P}{\partial r} = \rho \frac{v_\theta^2}{r} \quad (2)$$

The balance between the centrifugal force and the pressure gradient on a fluid element is given in Equation (1). Upon neglecting the higher order terms and considering the tangential velocity to be independent of the azimuthal position,  $\theta$ , we arrive at Equation (2).

Considering a Rankine vortex model to be a fit for the azimuthal velocity,  $v_\theta$ , whose radius is  $a$ , we have the following expressions for pressure in the outer region, where  $r > a$ .

$$\int_r^\infty dP = \int_r^\infty \rho \frac{V_\theta^2}{r^*} dr^* = \rho \left(\frac{\Gamma}{2\pi}\right)^2 \int_r^\infty r^{*-3} dr^* = \frac{\rho}{2} \left(\frac{\Gamma}{2\pi}\right)^2 (r^{*-2})|_r^\infty \quad (3)$$

$$P_\infty - P_r = \frac{\rho}{2} \left(\frac{\Gamma}{2\pi r}\right)^2 : r > a \quad (4)$$

Here  $P_\infty$  is the fluid pressure at a location far away from the fluid element in the vortex core. For the vortex core region, where  $r \leq a$ , we have the following pressure distribution:

$$\int_r^a dP = \int_r^a \rho \frac{V_\theta^2}{r^*} dr^* = \rho \left(\frac{\Gamma}{2\pi a^2}\right)^2 \int_r^a r^* dr^* = \frac{\rho}{2} \left(\frac{\Gamma}{2\pi a^2}\right)^2 (a^2 - r^2) \quad (5)$$

$$P_a - P_r = \frac{\rho}{2} \left(\frac{\Gamma}{2\pi a}\right)^2 - \frac{\rho}{2} \left(\frac{\Gamma}{2\pi a}\right)^2 r^2 : r \leq a \quad (6)$$

In the above expressions, we have the velocity distribution for the Rankine vortex model is as shown below:

$$V_\theta(r) = \frac{\Gamma}{2\pi a^2} r : r \leq a \quad (7)$$

$$V_\theta(r) = \frac{\Gamma}{2\pi r} : r > a \quad (8)$$

We have the equation for the pressure distribution as follows:

$$\begin{aligned} P_r &= P_\infty - \frac{\rho}{2} \left(\frac{\Gamma}{2\pi r}\right)^2 \\ &= P_a + \frac{\rho}{2} \left(\frac{\Gamma}{2\pi a^2}\right)^2 r^2 - \frac{\rho}{2} \left(\frac{\Gamma}{2\pi a}\right)^2 \end{aligned} \quad (9)$$

At the vortex radius,  $a$ , we have the pressure expressed as,

$$\begin{aligned} P_{r=a} &= P_\infty - \frac{\rho}{2} \left(\frac{\Gamma}{2\pi a}\right)^2 = P_a + \frac{\rho}{2} \left(\frac{\Gamma}{2\pi a^2}\right)^2 a^2 - \frac{\rho}{2} \left(\frac{\Gamma}{2\pi a}\right)^2 \\ \therefore P_a &= P_\infty - \frac{\rho}{2} \left(\frac{\Gamma}{2\pi a}\right)^2 \end{aligned} \quad (10)$$

The pressure at the center of the vortex ( $r = 0$ ) is minimum and it is given as,

$$\begin{aligned} P_{min} = P_{r=0} &= P_a - \frac{\rho}{2} \left(\frac{\Gamma}{2\pi a}\right)^2 \\ &= P_\infty - \frac{\rho}{2} \left(\frac{\Gamma}{2\pi a}\right)^2 - \frac{\rho}{2} \left(\frac{\Gamma}{2\pi a}\right)^2 = P_\infty - \rho \left(\frac{\Gamma}{2\pi a}\right)^2 \end{aligned} \quad (11)$$

The above expressions can be used to arrive at an expression for the cavitation inception number,  $\sigma_i$ .

$$-C_p = \frac{P_\infty - P_v}{\frac{1}{2} \rho V_\infty^2} = \left(\frac{\Gamma}{2\pi a V_\infty}\right)^2 = k \left[\frac{\Gamma}{a V}\right]^2 = \sigma_i \quad (12)$$

This can be written in terms of mid-span bound circulation and turbulent boundary layer thickness as,

$$\begin{aligned}\sigma_i &= k \left[ \frac{\Gamma/\Gamma_0}{a/\delta} \right]^2 \left[ \frac{\Gamma_0}{v\delta} \right]^2 = k \left[ \frac{\Gamma/\Gamma_0}{a/\delta} \right]^2 \left[ \frac{\frac{1}{2}C_L V c}{V \delta} \right]^2 = k \left[ \frac{\frac{1}{2}\Gamma/\Gamma_0}{a/\delta} \right]^2 \left[ \frac{\frac{1}{2}C_L}{0.37 R n^{-0.2}} \right]^2 \\ &= k \left[ \frac{\Gamma/\Gamma_0}{0.74(a/\delta)} \right]^2 C_L^2 R n^{0.4}\end{aligned}\quad (13)$$

In the above expression, vortex strength is defined as, the mid-span bound circulation as,  $\Gamma_0 = 1/2C_L V c$  and  $\delta/c = 0.37[Vc/v]^{-0.2} = 0.37/Rn^{0.2}$ . McCormick's expression for the cavitation inception number,  $\sigma_i$  by assuming that the vortex core radius in the vicinity of the wing tip is proportional to the pressure side turbulent boundary layer thickness as shown in Equation (13).

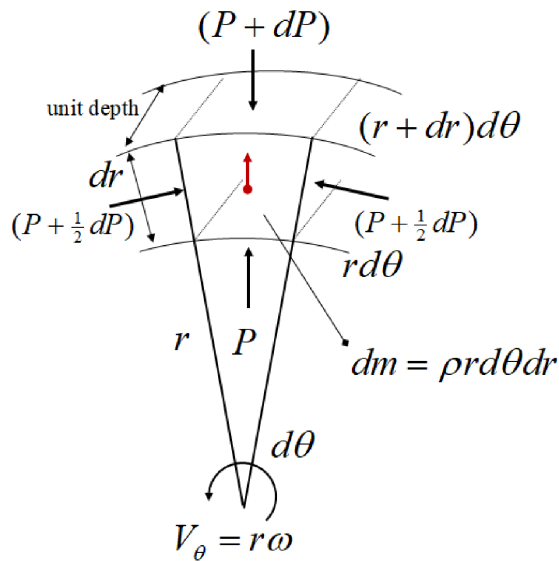


**Figure 5.** Schematic of the fluid element of mass,  $dm$  swirling about the vortex axis at the rate,  $\omega$ . The fluid element is in radial equilibrium by the balance between the pressure force and centrifugal force acting on it.

A three-component dynamometer was used to measure the lift coefficient of the hydrofoil at various combinations of angles of inclination and Reynolds number for NACA 16-020 and NACA 66(2)-415 elliptical hydrofoil to establish a scaling for the cavitation inception number. It was found from the measurements for the two hydrofoils that the cavitation inception number,  $\sigma_i$  adhered to the power-law relation (Equation (13)) given by McCormick. A linear fit between the cavitation inception number and the power-law relation is seen in Figure 6 for both NACA 16-020 and NACA 66(2)-415 elliptical hydrofoils used in the present experiments. A comparison between the experiments of maines [13] for NACA 16-020 and NACA 66(2)-415 hydrofoils are also shown as open squares and circles in Figure 6.

### 3.2. Cavitation Induced Noise

Tip vortex cavitation is generally associated with the streaks of water vapour issuing from the tip of three-dimensional hydrofoil with intense noise. The evolution of the wing tip cavitation with the decrease of the cavitation number is seen in six panels shown in Figure 7 for the elliptical planform NACA 16-020, at the angle of inclination,  $\alpha = 15^\circ$ . With the decrease in the cavitation number, six different stages were observed according to the cavitation number. They are shown as six frames from the top to the bottom in Figure 7: (1) Tip Vortex Cavitation (TVC) inception, (2) fully developed tip vortex cavitation, (3) attached tip vortex cavitation to the tip, (4) tip vortex cavitation with leading edge sheet

cavity, (5) tip vortex cavitation with cloud cavity and (6) tip vortex cavitation breakdown. The frequency response curve (sound pressure level vs frequency) obtained by performing Fast Fourier Transform (FFT) of the raw pressure signals from the unsteady pressure transducer corresponding to these six stages are in figures Figure 8. At the inception of cavitation, no peaks were observed in the frequency spectrum, when the tip vortex cavitation becomes fully developed at  $\sigma = 2.44$ , frequency peaks begin to appear in the power spectrum in Figure 8. Upon further decrease of the cavitation number, the frequency peak becomes strong at 1.1 KHz, with a strong Sound Pressure Level of about 150 dB. With further decrease of the cavitation number to  $\sigma = 2.14, 1.89 \& 1.66$ , the tip vortex cavitation with leading edge cavity appears, followed by tip vortex cavitation with cloud cavity and finally the break down of the tip vortex cavitation with fully developed cloud cavity in successive stages. However, in all these three stages at  $\sigma = 2.14, 1.89 \& 1.66$ , no clear noise peak is observed in the frequency spectrum. As shown in Figure 2, the cavitation inception corresponding to stage (1) is characterized by sporadic issuance of water vapor bubble packets along the vortex core. No peak is evident in the frequency spectrum at the stage (1) at  $\sigma = 6.49$  in Figure 9. With the further decrease of the cavitation number, the cavity along the core becomes stronger in the stage (2) and a mild noise peak can be seen in the frequency response curve at  $\sigma = 2.44$ . When  $\sigma = 2.29$ , the cavity at the tip of the hydrofoil gets attached to the hydrofoil and a specific frequency of about 1 kHz occurs at the stage (3), with the sound pressure level being closer to 150 dB in Figure 9. Upon further decrease of the cavitation number to  $\sigma = 2.29$ , the noise peak is seen to be not concentrated at about the 1kHz. However, the SPL values remain larger than the non-cavitating case with the decrease of cavitation number. At the stage (4) when  $\sigma = 2.14$ , a sheet cavity can be seen around the leading edge of the hydrofoil along with the attached tip vortex cavitation. Upon further decrease of the cavitation number in the stage (5), a cloud cavity is seen in the leading edge of the hydrofoil along with the tip vortex cavitation. In the stage (6), tip vortex cavitation begins to breakdown at the lowest value of the cavitation number. However, in stage (5) and stage (6), there is no clear concentrated peak frequency in the power spectrum in Figure 9.

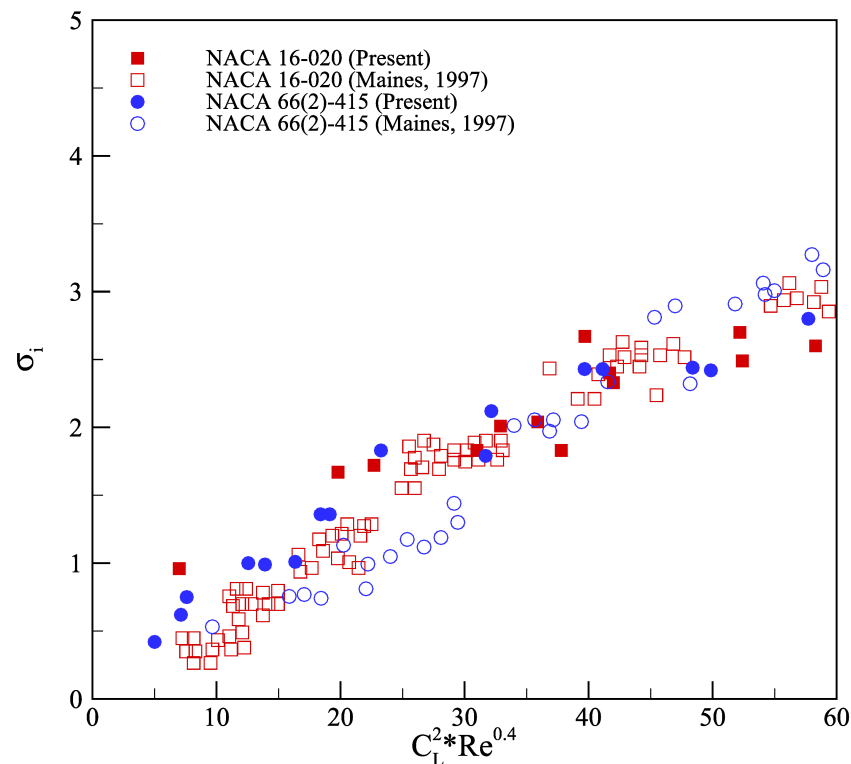


**Figure 6.** Cavitation inception scaling with the measured lift coefficient,  $C_L$  and Reynolds number,  $Re$ .

As opposed to NACA 16-020 hydrofoil, NACA 66(2)-415 hydrofoil, being an asymmetric hydrofoil, has an attached cavitation inception as shown in Figure 10 at  $\alpha = 8^\circ$ ,  $\sigma = 2.14$ . With the decrease in cavitation number, TVC in NACA 66(2)-415 undergoes an inception, cavity gets attached to the tip of the hydrofoil when  $\sigma = 1.89$  for the hydrofoil at  $\alpha = 8^\circ$ . A strong noise peak is visible around 1 kHz frequency as in Figure 9. With the further decrease of the cavitation number, sheet cavity and cloud cavities were formed at  $\sigma = 1.37$ ,  $\sigma = 1.28$ , respectively. It is observed from the frequency response curves that the noise associated with the cavitation increases in magnitude as seen by comparison with the non-cavitating case in Figure 9. Upon the comparison of the frequency response curves for NACA 16-020 and NACA 66(2)-415, a strong peak is seen around 1 kHz for both NACA 16-020 and NACA 66(2)-415 hydrofoils when the tip vortex cavitation gets fully attached to the hydrofoil as in Figure 11. This attachment of the tip vortex cavitation to the hydrofoil happens at  $\alpha = 15^\circ$  and  $\sigma = 2.29$  for NACA 16-020 and at  $\alpha = 8^\circ$  and  $\sigma = 1.66$  for NACA 66(2)-415.

Maines [16] described this noise occurring at a unique frequency as a vortex “singing”. However, the physical mechanism of this phenomenon is still not completely known and it is presumably due to the swirl of the standing wave on the water-vapor interface of the tip vortex cavity [20].

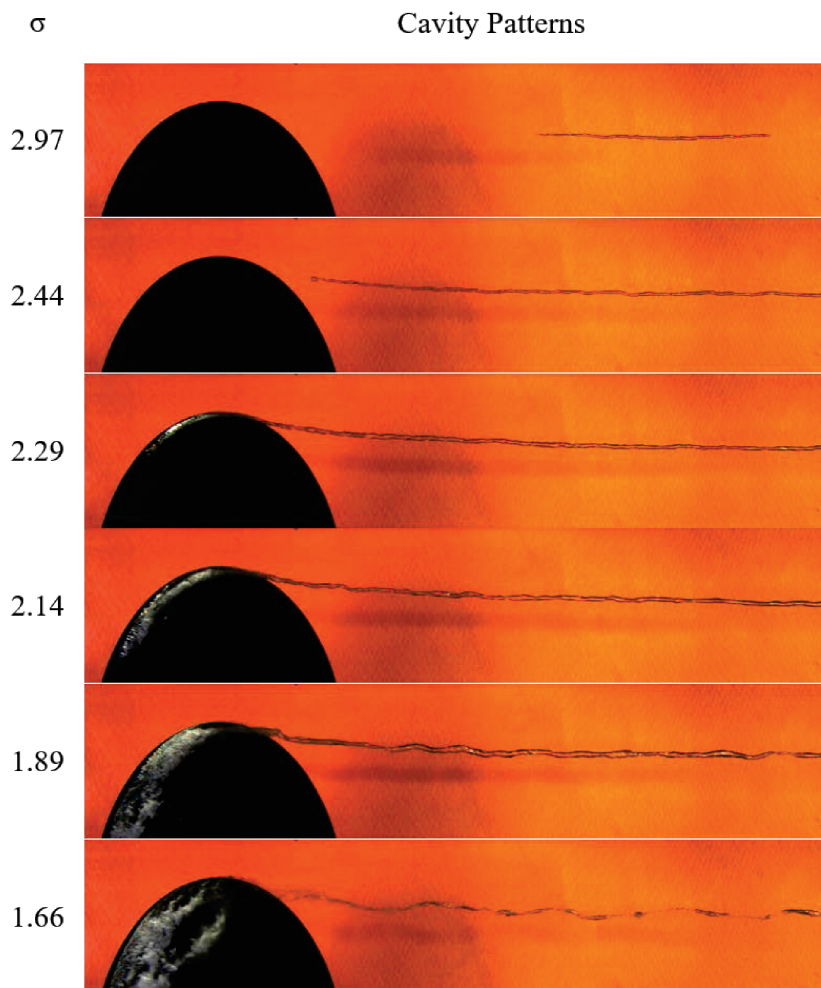


**Figure 7.** Cavitation pattern for NACA 16-020 hydrofoil at  $\alpha = 15^\circ$ .

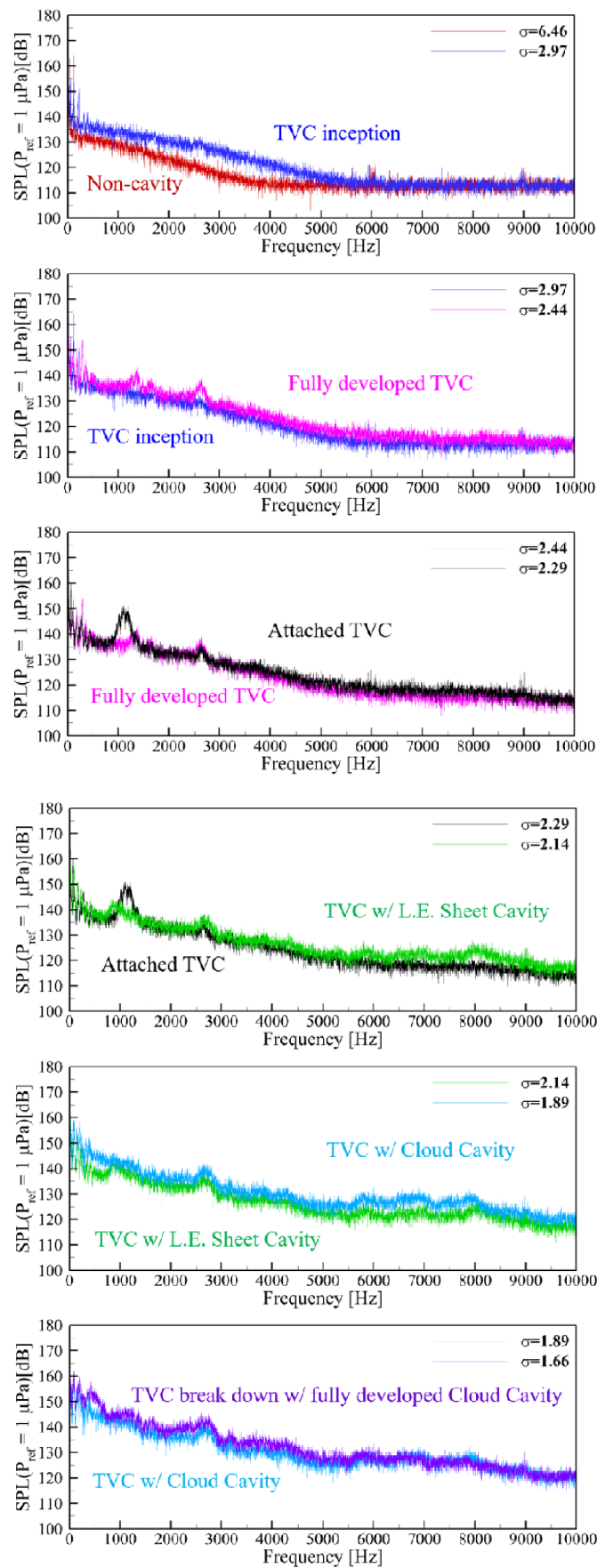
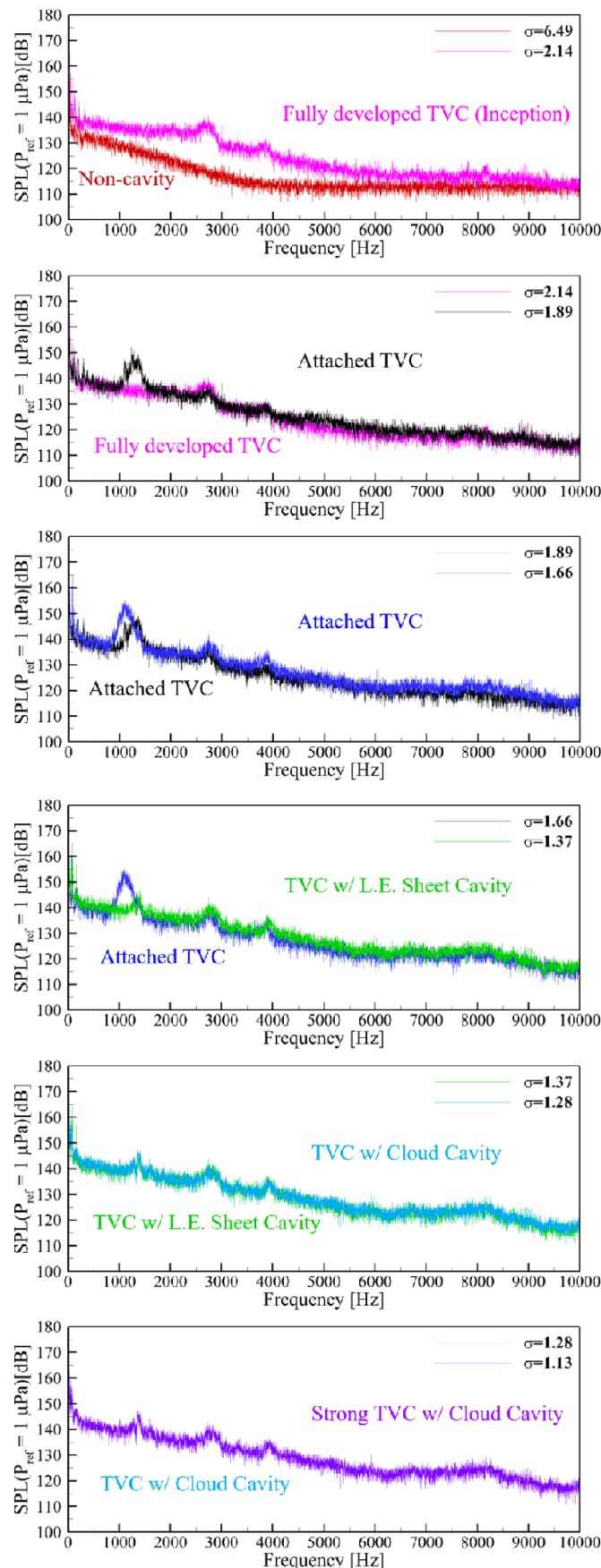
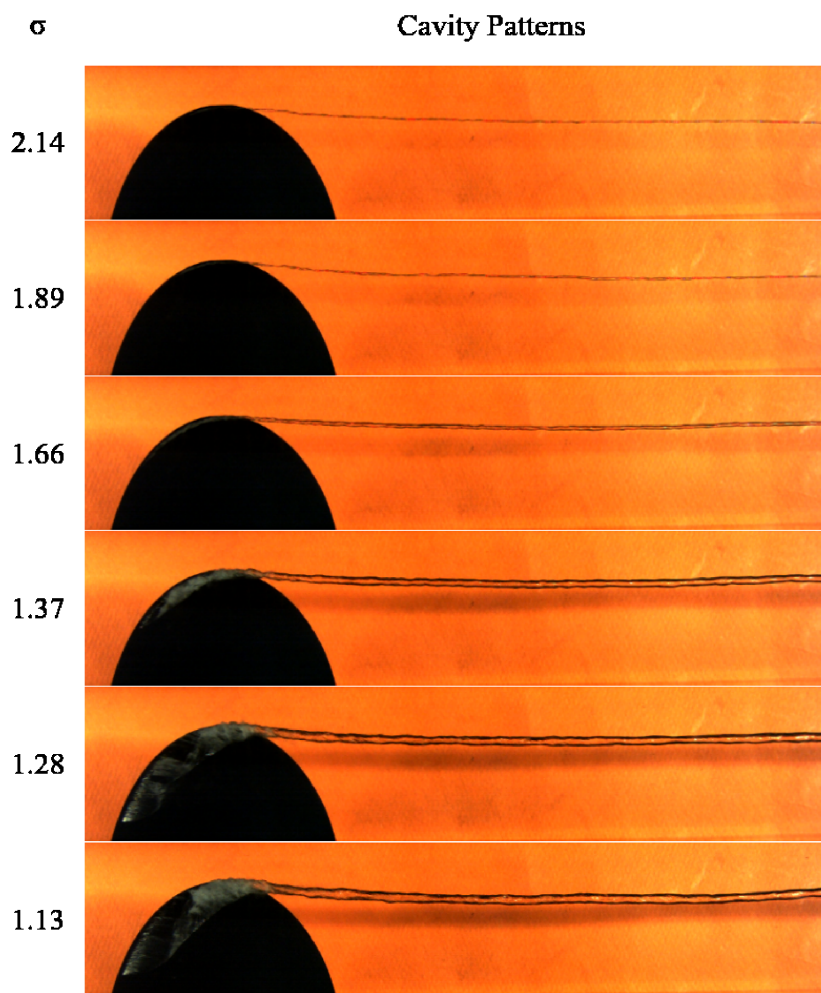


Figure 8. Induced noise characteristics of NACA 16-020 hydrofoil at  $\alpha = 15^\circ$ .



**Figure 9.** Induced noise characteristics of NACA 66(2)-415 hydrofoil at  $\alpha = 8^\circ$ .



**Figure 10.** Cavitation pattern for NACA 66(2)-415 at  $\alpha = 8^\circ$ .

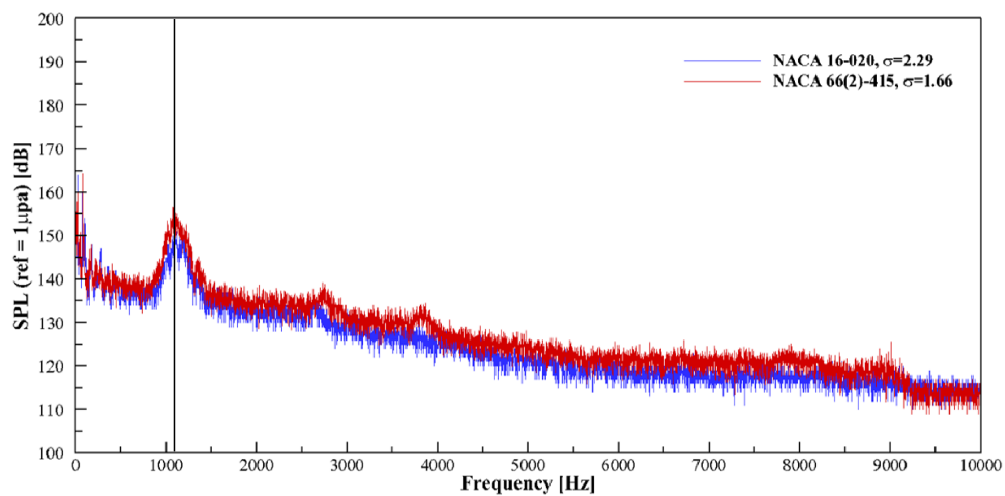


**Figure 11.** Comparison of noise characteristics of TVC attached to the tip of the hydrofoils.

#### 4. Conclusions

Experimental observations in relation to the inception of tip vortex cavitation and the induced noise characteristics from hydrofoils of elliptic planform (NACA 16-020 and NACA 66(2)-415) have been presented. Using a high-speed imaging, we identified the cavitation inception number for a given hydrofoil once the sporadic streaks of water vapour pockets appear in the vortex core. Upon the decrease of the cavitation number, the cavitation in the

vortex core became fully developed and got attached to the tip and further formed as sheet cavity and cloud cavity at the leading edge of the hydrofoil. The development process of tip vortex cavitation including inception is shown to occur in six different stages. Noise due to the cavitation was measured by unsteady pressure sensors. It was found that the sound pressure levels associated with the cavitating case was found to be considerably higher than the non-cavitating case. It was also found that there was an intense noise with a discrete frequency as the cavitating vortex grows and gets attached to the tip of the hydrofoil.

**Author Contributions:** Conceptualization and methodology, S.S. and B.-K.A.; investigation, S.S., J.-W.H. and D.N.; writing—S.S.; writing—review and editing, supervision, B.-K.A.; project administration and funding acquisition, S.-G.P. All authors have read and agreed to the published version of the manuscript.

**Funding:** This work was supported by the National Research Foundation of Korea (NRF) grant funded by the Korea government (MSIT) (No. 2019R1A2C1084306) and Daewoo Shipbuilding & Marine Engineering Co., Ltd.

**Institutional Review Board Statement:** Not applicable.

**Informed Consent Statement:** The study did not involve humans.

**Data Availability Statement:** The data presented in this study are available on request from the corresponding author.

**Acknowledgments:** We thank National Research Foundation of Korea (NRF) of the Korean government and Daewoo Shipbuilding & Marine Engineering Co., Ltd. for the funding.

**Conflicts of Interest:** The authors declare no conflict of interest. The funders had no role in the design of the study; in the collection, analyses, or interpretation of data; in the writing of the manuscript, or in the decision to publish the results.

## Abbreviations

The following abbreviations are used in this manuscript:

TVC	Tip Vortex Cavitation
SPL	Sound Pressure Level
LDV	Laser Doppler Velocimetry
SPIV	Stereo Particle Imaging Velocimetry
CMOS	Complementary metal–oxide–semiconductor
FFT	Fast Fourier Transform

## References

1. Burrill, L.C. Sir Charles Parsons and cavitation. *Inst. Mar. Eng. Trans.* **1951**, *LXIII*, 149–167.
2. Peng, X.X.; Xu, L.H.; Liu, Y.W.; Zhang, G.P.; Cao, Y.T.; Hong, F.W.; Yan, K. Experimental measurement of tip vortex flow field with/without cavitation in an elliptic hydrofoil. *J. Hydodyn. Ser. B* **2017**, *29*, 939–953. [[CrossRef](#)]
3. Jeong, N.-G. Three-Dimensional Analysis of the Turbulent Wingtip Vortex Flows of a Wing with NACA 16-020 Airfoil Section. *Trans. Korean Soc. Mech. Eng. B* **2009**, *33*, 635–642. [[CrossRef](#)]
4. Fruman, D.H.; Cerrutti, P.; Pichon, T.; Dupont, P. Effect of hydrofoil planform on tip vortex roll-up and cavitation. *J. Fluids Eng.* **1995**, *117*, 162–169. [[CrossRef](#)]
5. Bosschers, J. Propeller Tip-Vortex Cavitation and Its Broadband Noise. Ph.D. Thesis, University of Twente, Enschede, The Netherlands, 2018. Print Service Ede BV.
6. Arakeri, V.H. Cavitation inception. *Proc. Indian Acad. Sci. Sect. C Eng. Sci.* **1979**, *2*, 149–177.
7. Astolfi, J.-A.; Fruman, D.H.; Billard, J.-Y. A model for tip vortex roll-up in the near field region of three-dimensional foils and the prediction of cavitation onset. *Eur. J. Mech. B/Fluids* **1999**, *18*, 757–775. [[CrossRef](#)]
8. Arndt, R.E.; Keller, A.P. Water quality effects on cavitation inception in a trailing vortex. *J. Fluids Eng.* **1992**, *114*, 430–438. [[CrossRef](#)]
9. Briancon-Marjollet, L.; Merle, L. Inception, Development and Noise of a Tip Vortex Cavitation. Available online: <https://www.nap.edu/read/5870/chapter/59/> (accessed on 1 May 2021)
10. McCormick, B.W., Jr. On cavitation produced by a vortex trailing from a lifting surface. *J. Fluids Eng.* **1962**, *84*, 369–378. [[CrossRef](#)]

11. Souders, W.G.; Platzer, G.P. (David W Taylor Naval Ship Research and Development Center Bethesda MD). 1981. Available online: <https://apps.dtic.mil/sti/citations/ADA098297> (accessed on 1 May 2021)
12. Billet, M.L.; Holl, J.W. Scale effects on various types of limited cavitation. *J. Fluids Eng.* **1981**, *103*, 405–414. [[CrossRef](#)]
13. Maines, B.H.; Arndt, R.E. Tip vortex formation and cavitation. *J. Fluids Eng.* **1997**, *119*, 413–419. [[CrossRef](#)]
14. Keller, A.P. Cavitation Scale Effects-Empirically Found Relations and the Correlation of Cavitation Number and Hydrodynamic Coefficients. Technische Universität München. Available online: <https://resolver.caltech.edu/CAV2001:lecture.001> (accessed on 1 May 2021).
15. Higuchi, H.; Arndt, R.E.A.; Rogers, M.F. Characteristics of tip vortex cavitation noise. *J. Fluids Eng.* **1989**, *111*, 495–501. [[CrossRef](#)]
16. Maines, B.; Arndt, R.E. The case of the singing vortex. *J. Fluids Eng.* **1997**, *119*, 271–276. [[CrossRef](#)]
17. Choi, J.-K.; Chahine, G.L. Noise due to extreme bubble deformation near inception of tip vortex cavitation. *Phys. Fluids* **2004**, *16*, 2411–2418. [[CrossRef](#)]
18. Pennings, P.; Westerweel, J.; van Terwisga, T. Cavitation tunnel analysis of radiated sound from the resonance of a propeller tip vortex cavity. *Int. J. Multiph. Flow* **2016**, *83*, 1–11. [[CrossRef](#)]
19. Peng, X.; Wang, B.; Li, H.; Xu, L.; Song, M. Generation of abnormal acoustic noise: Singing of a cavitating tip vortex. *Phys. Rev. Fluids* **2017**, *2*, 053602. [[CrossRef](#)]
20. Bosschers, J. Investigation of the resonance frequency of a cavitating vortex. In Proceedings of the NAG/DAGA International Conference on Acoustics, Rotterdam, The Netherlands, 23–26 March 2009.